Submitted Version

Performance and dynamic behaviour of FRP strengthened CFST members subjected to lateral impact

Md IftekharulAlam[a], Sabrina Fawzia[a,*], Xiao-Ling Zhao[b], Alex M. Remennikov[c],M.R. Bambach[d], M. Elchalakani[e]

[a]*School of Civil Engineering and Built Environment, Science and Engineering Faculty, Queensland University of Technology (QUT), 2 George Street, Brisbane, QLD 4000, Australia*

[b]*Department of Civil Engineering, Monash University, Clayton, Victoria 3800, Australia*

[c]*School of Civil, Mining and Environmental Engineering, University of Wollongong, Wollongong, NSW 2522, Australia.*

[d]*Department of Civil Engineering, The University of Sydney, Sydney, Australia.*

[e]*The School of Civil, Environmental and Mining Engineering at the Faculty of Engineering, Computing and Mathematics, the University of Western Australia, Australia.*

(*Corresponding Author: sabrina.fawzia@qut.edu.au Tel: 61 7 3138 1012 Fax: 61 7 3138 1170)

Email addresses: sabrina.fawzia@qut.edu.au (S. Fawzia), mdiftekharul.alam@hdr.qut.edu.au (M. I. Alam), ZXL@monash.edu (X.-L. Zhao), alexrem@uow.edu.au (A. Remennikov), M.R. Bambach (mike.bambach@sydney.edu.au), M. Elchalakani (mohamed.elchalakani@uwa.edu.au)

ABSTRACT

Due to the increasing popularity of concrete-filled steel tubular (CFST) members, there will be more chances of vehicles/vessels or terrorist attacks on these structures in near future. Fibre-reinforced polymer (FRP) strengthening can be an effective option to reduce impact damage or failure of CFST members. However, existing knowledge is very limited in understanding the behaviour of FRP strengthened CFST structures under lateral impact loading. This paper outlines drop hammer impact test results of a series of experimental programs of bare and FRP strengthened CFST specimens. A total of sixteen CFST specimens were prepared and tested under lateral impact at their mid-span. The results indicate that permanent lateral displacement of CFST members can be reduced up to 18.2% by externally

bonded FRP sheets. The effects of FRP type, FRP wrapping direction, carbon fibre-reinforced polymer (CFRP) wrapping layers, wrapping length, and impact velocity were investigated to understand the influences of these parameters on the behaviour of strengthened CFST specimens. CFRP laminates were found to be weak under impact loading when wrapped in only longitudinal direction. However, a combination of longitudinal and hoop layers of CFRP laminates, or only GFRP wrapping, can remarkably minimise the severity of damage and failure of FRP in CFST specimens under lateral impact. A comparison of current test results with recent works has been presented to understand the effect of impact energy on the lateral displacement control ability of FRP strengthened CFST members.

Keywords: Concrete-filled steel tubular (CFST) members, lateral impact, fibre-reinforced polymer (FRP), dynamic loading.

Nomenclature

H	Impactor height
F_p	Peak impact force
F_r	Residual impact force
δ_p	Peak lateral displacement
δ_r	Residual lateral displacement
$CFRP_{Test}$	Epoxy cured CFRP laminate properties obtained from test
$GFRP_{Test}$	Epoxy cured GFRP laminate properties obtained from test

1. Introduction

The application of concrete-filled steel tubular (CFST) structures has been growing rapidly in the construction industry. The faster construction and superior mechanical properties are the major advantages of these members over the reinforced concrete (RC) structures. In recent years, CFST members have been a very popular choice to use, not only as structural columns, but also in other forms of structural components such bridge girders, utility transmission

towers [1], and jacket legs and braces of offshore structures where axial static force is very low or negligible. Lateral impact forces may be expected on these members from transportation accidents, explosive attacks or from flying debris. Lateral impact loads can cause significant damage or failure of CFST members, if they are not designed to withstand these external imposed actions. A suitable strengthening technique needs to be developed to protect these CFST members where lateral impact force is more likely to be expected.

The fibre-reinforced polymer (FRP) wrapping of RC structures using high strength structural epoxy adhesives is a proven technique to enhance the capacity of the RC structural members. However, compared to the RC structures, literature is limited on the behaviour of FRP strengthened steel and steel-concrete composite structures. Over the last decade, researchers in the field of structural engineering have given their attention to investigating the effectiveness of FRP strengthening of metallic structures. A good number of studies have been conducted to understand the joint behaviour between carbon-fibre reinforced polymer (CFRP) sheets and steel plates under both static and dynamic loads [2-10]. Strengthening of different hollow steel structures using CFRP sheets and plates under static loadings has showed great potential from experimental and numerical observations [11-21]. The performance of CFRP strengthened square hollow section (SHS) steel columns under lateral impact loading was investigated by Alam et al. [22, 23]. Very recently lateral impact tests of FRP strengthened circular hollow-section (CHS) steel members were conducted to understand the failure modes and effect of FRP wrapping of strengthened members [24].

The axial compressive load enhancement of CFRP strengthening of CFST columns was noticed in early studies [25-32]. A number of recent works have shown that CFST columns provided improved impact resistance capacities compared to hollow tubular columns [33-36]. Thus, further strengthening of the CFST column can be a promising composite member to safely carry both axial static and lateral impact loads. In addition to that, FRP strengthening is

highly effective to prevent corrosion of outer steel surfaces in sea water and any harsh environments. However, research of CFRP wrapped CFST columns subjected to lateral impact is very limited. Chen et al. [37] conducted drop mass impact testing of CFRP and glass-fibre reinforced polymer (GFRP) strengthened CFST columns. GFRP wrapping was found to be successful to minimise lateral displacement up to 50% of that of the bare specimen. Another very recent experimental research work has also confirmed that CFRP wrapping helped to increase the stiffness of strengthened CFST members subjected to falling mass impact [38]. The Finite Element (FE) numerical models of CFRP wrapped CFST columns were developed and validated in another study [39]. The results showed that that after a certain bond length, any further extension of the wrapping length had a negligible or no effects on the deflection of CFST columns [39]. To examine the effect of a realistic vehicular impact, full-scale CFRP strengthened columns with a simplified vehicle model were previously developed [40, 41]. The results of the analyses have shown that full CFST columns in low-rise buildings are vulnerable under vehicular impact loading with a vehicle speed of 90 km/h or more. Also it was shown that, CFRP wrapping can successfully prevent the failure of CFST columns by providing additional tensile capacity from the tension face of the columns [40].

It is very important to understand the actual structural responses and dynamic failure behaviour of FRP strengthened CFST members under lateral impact through experimental tests. In the study of Chen et al. [37], the plastic deformations of the specimens were not significant due to low impact energy. Thus, it was not possible to understand the failure mechanism of FRP laminates after the tests. Moreover, the impactor and FRP wrapped specimens were not in direct contact due to the steel plate clamping at the impact zone and the actual failure modes of FRP strengthened specimens at impact location were unknown. In the case of Shakir et al. [38], they only considered one CFRP layer with one-third of the span

length. According to the current knowledge of the authors, none of the above experimental works explicitly investigated the failure pattern of wrapped FRP sheets in CFST specimens depending on the FRP type, wrapping orientation and FRP thickness as well as the effect of different wrapping lengths. In summary, the difference of the current work described in this paper and prior works includes (i) sufficient impact energy is employed to produce plastic deformation in the specimens, (ii) test set up to ensure direct contact of impactor and FRP wrapped specimens so that local failure can be investigated, (iii) wide range of parameters are considered such as FRP type, wrapping orientation, FRP thickness and FRP bond length. Therefore, this paper aims to investigate the failure behaviour of FRP sheets and the structural responses of bare and strengthened CFST members against lateral impact by considering the above parameters (FRP type, wrapping orientation, FRP thickness and FRP bond length) to better understand the dynamic behaviour of such strengthened structures. A total of 16 specimens were tested with the combination of bare, CFRP and GFRP strengthened CFST members. The results are presented in terms of lateral displacement, impact force and failure modes of CFST and FRP sheets. The effects of different governing parameters were investigated followed by comparison of present results with early studies.

2. Experimental program

2.1 Materials properties

Five different materials: concrete, steel, CFRP, GFRP and epoxy adhesive were used in this research to prepare the FRP strengthened CFST specimens. The core concrete was supplied by Hymix Australia Pty Ltd with a maximum aggregate size and nominal compressive strength of 10 mm and 25 MPa, respectively. Five concrete cylinders of 100 mm in diameter and 200 mm in length were prepared according to the AS1012.9 [42] to determine unconfined compressive strength of the concrete sample. Another three cube specimens with dimensions of$100\,mm \times 100\,mm \times 350\,mm$ were cast as specified in AS 1012.8.2:2014

[43] to obtain the tensile properties of the concrete by flexure testing. The compression tests were performed using a 2000 kN Instron universal testing machine as shown in Fig. 1(a). An axial extensometer with 150 mm gauge length was used to accurately measure the axial strains of the specimens (Fig. 1(a)). The four-point bending test setup of the concrete cube sample is displayed in Fig. 1(b). The average unconfined compressive strength and tensile flexure strength of concrete within a week of impact test were 29.7 MPa and 4.2 MPa, respectively. Cold-formed steel pipes of 6500 mm length were cut to 1600 mm length circular hollow section (CHS) steel tubes for specimen preparation. The outer diameter and wall thickness of tubular specimens were 114.3 mm and 4.5 mm, respectively. The specimens were supplied by OneSteel Limited, Australia, and manufactured as Grade C250L conforming to AS 1163 [44]. The standard steel coupons were fabricated from CHS steel tubes according to AS 1391 [45] to obtain the mechanical properties of the steel material. The average elastic modulus, tensile strength, and yield stress were 211 GPa, 366 MPa and 317 MPa, respectively. CFRP material used for the strengthening purpose was supplied by BASF Construction Chemicals Australia Pty Ltd. The CFRP sheets were commercially known as MBrace Fib 300/50 CFS. The unidirectional GFRP composite sheets used in this study were provided by CG Composites Australia Pty Ltd. The material properties of epoxy-cured CFRP and GFRP laminates were obtained through tensile coupon tests. The tensile coupon test was conducted according to ASTM D3039-08 [46]. The details of test setup for both CFRP and GFRP coupon tests are shown in Fig. 2. MBrace 4500 epoxy adhesive and MBrace 3500 adhesion promoter primer were used to achieve bonding between the steel surface and the FRP sheets. Both of them were two parts epoxy-based resins and provided by BASF Construction Chemicals Australia Pty Ltd. The average static measured material properties of the same epoxy adhesive were obtained by Kabir et al. [17] through standard tensile coupon

tests. The mechanical properties of CFRP and GFRP laminates and epoxy adhesive are listed in Table 1.

2.2 Specimen preparation

The first step in the specimen preparation was to strengthen the CHS steel tubular specimen with adhesively bonded CFRP and GFRP sheets. Initially, the outer surfaces of the tubular members were prepared by sand blasting to remove impurities from the steel surface. Early research works have shown that grit and sand blasting surface preparation techniques are effective in achieving good bonding between the FRP and the outer surface of steel [18, 47-49]. Fig. 3(a) shows the specimens after sand blasting. The sand blasted specimens were cleaned with acetone to remove dust from the steel surface before starting the strengthening process. At the beginning of the FRP strengthening process, MBrace 3500 primer was applied on the cleaned sand blasted specimens' surfaces according to the manufacturer guidelines. A recent study has shown that treating with epoxy-based adhesion promotion primer can enhance the strength of CFRP wrapped specimens compared to the non-treated specimens [18]. The MBrace 4500 two-part adhesive was mixed properly and applied on top of the primer-treated specimens. Then the FRP sheets with required sizes were wrapped on the treated steel surfaces. The rib-rolling was carried out to fully saturate the FRP fibres, which helped to form epoxy/FRP laminates with uniform thickness. Fig. 3(b) displays the rib-rolled FRP wrapped specimens ready for curing. After rib-rolling in wet conditions, the specimen was wrapped with a masking tape and cured for 24 hours to prevent premature debonding. After that, the strengthened specimens were allowed to cure for at least two weeks prior to make them ready for concrete filling. The steel plates with 10 mm thickness were fabricated to confine the base of the specimens by welding, as shown in Fig. 3(c). The strengthened tubular members were filled with concrete in layers and vibrated using a poker vibrator (Fig. 3(d)). The concrete filling and compaction were performed carefully to avoid

any damage of outer FRP layers due to vibration of freshly poured concrete. Then the filled specimens were covered by polythene sheets to allow the compete hydration of concrete.

2.3 Experimental program details

A total of sixteen specimens were prepared to conduct drop hammer impact tests. Thirteen specimens were strengthened and the rest of the three were kept as bare specimens. The FRP wrapped members were classified based on FRP type, wrapping direction, wrapping length, number of FRP layers, and impact velocity. The specimen label consists of three parts: in the first part, CFT represents concrete-filled tube specimen, CCFT represents the CFRP strengthened concrete-filled tube specimen, GCFT represents the GFRP strengthened steel specimen, and GCCFT represents both GFRP and CFRP strengthened steel specimens. In the second part, B denotes as the bare specimen, L represents FRP wrapping in a longitudinal direction, H denotes FRP wrapping in a hoop direction. The number of CFRP layers is represented by the number of letters in the second part of each specimen label. For example, two FRP layers in a longitudinal direction are identified by LL, and HL means the first layer in a hoop direction, the second layer in a longitudinal direction and LHL means the first layer in the longitudinal direction, the second layer in the hoop direction and the third layer in the longitudinal direction. In the last part, the V1 and V2 in the last part denote the impact velocity of 5 m/s and 3.28 m/s, respectively. The specimen details and test matrix are listed in Table 2.

2.4 Test setup and procedure

The lateral impact tests were performed using the drop hammer impact testing facility at the University of Wollongong. The schematic diagram and detailed photographic view of the test setup are shown in Fig. 4. The total mass of the drop hammer machine was 592 kg consisting of a falling mass, dynamic load cell and the impactor (Fig. 4). The flat headed impactor was

cylindrical in shape with 100 mm of diameter and 50 mm height. The dynamic load cell with 1600 kN capacity was used to measure the contact forces between the specimens and the impactor. The mid-span displacement in the direction of loading was measured using a non-contact laser displacement measuring system. A high-speed camera was used for all the impact events to record the dynamic failure process of the bare and the strengthened specimens (Fig. 4(b)). A leveller was placed to track the deflection of the specimens (Fig. 4). A similar technique was used in recent research to measure the mid-span deflection of reinforced concrete beams [50] with GFRP rebar. The distance between the impactor and the specimen surface was varied from 550 mm to 1274 mm for obtaining initial drop hammer velocities of 3.28 m/s and 5 m/s, respectively. The high-speed data acquisition system with a frequency of 50,000 Hz was used to record all the experimental data. Support-to-support clear span was selected as 1300 mm. The impact position for all the specimens was at the mid-span and the support conditions were kept as simply support. Soft rubber bands were used to prevent the rebounding tendency of the specimens during the impact events, as shown in Fig. 4(b).

3. Experimental Results

3.1 Impact force time histories

Fig. 5 exhibits the impact force versus time curves from the drop hammer impact tests. The moment of contact of the specimen surface and the impactor is aligned with time = 0 s. A sharp rise of the impact force was noticed due to the interfacial resistance of the specimens. The specimens instantly accelerated to the velocity of the impactor from a stationary position at the time of the initial strikes by the impactor. The peak initial forces varied from 248.3 kN to 315.9 kN subjected to 5 m/s impact velocity as listed in Table 3. The difference of contact area, contact surface hardness and the complex contact behaviour between the impactor and

the outer surface of the specimens may cause the variation of initial peak impact force. A sudden drop of impact force from initial peak to zero was observed with rapid vibration for the first 5 to 6 milliseconds. The zero impact force may occur due to the short time separation of the impactor and the specimen surface. The similar kind of behaviour of hollow steel and CFST members under lateral impact was observed in both experimental and numerical studies [22, 35]. A plateau stage started after the vibration phase with a stable contact between the hammer head and the specimens until the rebound of the impactor. The flexure resistance capacity of the specimens under dynamic lateral impact loading is related to the average residual impact force developed in the plateau stage. The specimens started responding under lateral impact by global deformation in this stage, as revealed from the high speed camera records. After the peak lateral displacement, the forces started decreasing in the rebounding phase and reached zero at the time of separation of impactor from the specimens' surfaces.

3.2 Lateral displacement time histories

It was observed that due to the high impact energy and brittle behaviour of CFRP laminate, some of the specimens experienced large debonding and CFRP rupture at the tension face of the mid-span. Thus, the maximum range of the displacement laser sensor was reached as the debonded CFRP laminates separated from the specimens and travelled more than the actual displacement of the specimens. The lateral displacement time histories and image frames at the time of initiation of CFRP debonding of CCFT-LLL-V1 and CCFT-LHL-V1 members are shown in Fig.6. It was noticed that the time to reach the maximum laser sensor limit and the time of initiation of CFRP debonding were the same. Thus, debonding of CFRP was the cause of failure to record the actual displacements of the specimens using the displacement laser sensor. The displacement time histories of the specimens that reached their maximum sensor range were obtained using the image frames extracted from the high-speed video

records. The leveller and the tracking points (Fig. 6(b)) were used to extract frame-by-frame displacement data and then the corresponding displacement versus time records were plotted to obtain the lateral displacement time histories. The lateral displacement time histories obtained from the displacement laser sensor and the high speed camera of CFT-B-V1(1) and CFT-B-V2 were compared and a good agreement between the two displacement measuring systems was found, as shown in Fig. 7. The formation of relatively grey colour zones at the bottom of CCFT-LLL-V1 and CCFT-LHL-V1 (Fig. 7(b)) confirmed the debonding initiation at 0.016 s and 0.0192 s impact durations, respectively. The displacement responses of the specimens obtained from the laser sensor and the high speed camera are listed in Table 3.

Fig. 8 depicts the lateral displacement time histories of the bare and two layers CFRP strengthened CFST specimens in a longitudinal direction under lateral impact. CFRP wrapping showed improved impact resistance capacity by minimising both peak lateral and residual displacements compared to the bare specimens. The peak lateral displacement was reduced from 87 mm to 76.5 mm because of the CFRP wrapping (Table 3 and Fig. 8). The residual or permanent lateral displacement reduction could be achieved up to 18.2% of bare CFST member by two layers of GFRP wrapping.

3.3 Impact force versus lateral displacement

Fig. 9 illustrates the impact force-lateral displacement curves of the tested specimens. The residual forces (F_r) listed in Table 3 are obtained from Fig. 9 by considering the average force at the plateau stage. The residual forces of the specimens are almost similar, with maximum and minimum values of 82 kN and 92 kN respectively under 5 m/s impact velocity. However, residual forces of most of the strengthened members are higher than the corresponding bare members. This indicates the enhancement of dynamic bending strength of CFST members due to FRP wrapping.

3.4 Failure modes

Fig. 10 shows the high-speed video frames to examine the failure progress of bare and wrapped CFST specimens during the impact events. The high-speed camera footage of specimens' response at the impact locations are shown in Fig. 10. At the initial stage of impactor-specimen contact (t=0.0018 s), rapid vibration was noticed for all the specimens. The fast movement of the tracking points in Fig. 10(b) were because of the vibration of the specimens after initial peak impact force. These early vibration noises were also recorded in impact force-time curves (Fig. 5). The CFRP debonding and brakeage failure of a one-layer longitudinally wrapped CFRP strengthened specimen at the tension face of impact zone was observed at the beginning of the plateau stage (t=0.015 s).In an impact event, the specimens started reacting against the imposed loading in the plateau stage. Thus, the initiation of global deformation and CFRP failure was expected at this stage. However, a single layer CFRP wrapped member in the hoop direction exhibited no debonding failure at the tension face as shown in Fig. 10. The CFRP failure of the longitudinally wrapped specimen was more prominent at time instant t=0.042 s, as at that time specimens deflected to around the maximum peak deformation. CFRP fracture and cracks were also noticed at the compression face of the impact zone in both wrapped specimens. This is due to the brittle behaviour of CFRP laminate under dynamic compressive loading. The similar findings have also been reported in an early study of CFRP strengthened CFST members under lateral impact [37]. At t=0.07 s, the impactor separated from the specimens due to the rebounding effect. Fig. 5 also confirms that after t=0.05 s, impact forces of all the specimens were zero. The failure modes of bare and one-layer strengthened specimens are presented in Fig. 11. All the specimens exhibited global deformation failure at impact location. No local deformation was noticed in both compression and tension faces of the bare specimen. Similar failure mode of CFST specimens under static bending loading has been observed in a previous study [51]. A

specimen strengthened in a longitudinal direction showed fracture and fibre breakage at compression face and fibre breakage and debonding failure at tension face. The fibre breakage failure of CFRP was due to the large global deformation of the specimen. In case of one layer strengthened specimen in hoop direction, no fibre breakage was noticed as no specimens exhibited local outward buckling. However, CFRP laminate cracks or separations in transverse direction were observed, as presented in Fig. 11. Fig. 12 discloses the failure mode of core concrete of bare and strengthened specimens. The wider cracks were noticed for bare specimens because of larger lateral displacements, compared to the wrapped specimens. Furthermore, separation of core concrete was also found due to the larger cracks (Fig. 12). However, no concrete separation was noticed at the tension face of the wrapped specimen.

3.5 Energy absorption due to global deformation

The kinetic energy produced during a drop hammer impact test can be written as, $E_k = \frac{1}{2}MV^2$. Here, M and V are the total mass and the initial impact velocity of the impact hammer. This energy absorbed by the specimens is mainly due to global deformation and elastic rebounding of the specimens. The energy dissipated for the global deformation of the specimens was estimated using the energy absorption formula developed by Bambach [52]:

$$W_o = \frac{(CN_u)^2\delta_p^3}{6ABDM_uL} + \frac{8ABM_u\delta_p}{L} \quad (1)$$

here, A, B, C and D are the coefficients related to support end rotation, axial loads, axial translational restraint and specimen shape. The tensile capacity, bending moment, peak lateral displacement and support-to-support span (1300 mm) are denoted as N_u, M_u, δ_p and

L,respectively. The present experimental setup consisted of simply support ends condition without axial loading. Therefore, Eq. 1 can be rewritten as follows:

$$W_o = \frac{(8 \times 0.5) M_u \delta_p}{L} \quad (2)$$

The bending moments due to transverse impact at mid-span of the specimens were calculated from$M_u = (F_r \times L)/4$. It was also noticed that dynamic forces at the residual stage were nearly constant (Fig. 9). Thus, the average residual forces (Table 3) were considered as the dynamic capacity (F_r) of the specimens. The global deformation energies obtained from Eq. (2) are presented in Table 4. The percentage of the ratio of global deformation energy and kinetic energy varied between 93.8% and 85.1%. Therefore, the major portion of impact energy was dissipated due to global deformation of the specimens. The bare specimen absorbed more or equal impact energy by global deformation, due to larger lateral displacements than the strengthened specimens. The slight reduction of global energy dissipation of strengthened specimens might be due to the enhanced stiffness rather than their bare counterparts.

4. Results and Discussion

4.1 FRP type

To study the effects of different FRP types, both CFRP and GFRP sheets were used to strengthen CFST members. The lateral displacement-time histories and impact force-lateral displacement responses of CFRP, GFRP and a combination of CFRP and GFRP strengthened specimens are displayed in Fig. 13. It is interesting to note that two layers GFRP strengthened specimen in longitudinal direction has shown better performance by minimising peak lateral displacements to 75.1 mm. On the other hand, two layers CFRP wrapped specimens in

longitudinal direction exhibited 2% higher peak lateral displacement (Table 3 and Fig. 13) compared to the GFRP wrapped counterpart. First layer GFRP and second layer CFRP strengthened specimen showed almost similar peak displacement of GCFT-HL-V1. However, the residual displacements of CCFT-LL-V1, GCFT-LL-V1 and GCFT-HL-V1were nearly the same as, revealed in Fig. 13(a). Fig. 13(b) shows the impact force-lateral displacement comparison of CFRP and GFRP confined CFST members. The peak impact forces of GFRP wrapped specimens were higher than the CFRP wrapped specimens. This similar characteristic of increasing peak impact force of GFRP strengthened CFST members have also been found in an early study [37]. However, no significant difference in residual forces was noticed between two different FRP types. The failure modes of FRP wrapped specimens after drop hammer impact are presented in Fig. 14. The CCFT-LL-V1 specimen suffered severe CFRP breakage, fibre damage and debonding failure in both compression and tension faces of the impact zone. This is due to the highly brittle behaviour of CFRP laminates under impact loading. The GFRP strengthened members exhibited fibre damage at the compression face and fibre breakage at the tension face as displayed in Fig. 14. No significant debonding failure was noticed for GFRP wrapped specimens. Furthermore, the severity of fibre damage and breakage of GFRP laminates were remarkably less than the CFRP laminates. Thus, GFRP laminates exhibited superior impact resistance due to their improved toughness property compared to the CFRP laminates. The combination of first layer GFRP and second layer CFRP also contributed to minimise the debonding failure of CFRP laminates (Fig. 14). The comparison of core concrete failure modes of CFRP and GFRP wrapped specimens are shown in Fig. 12. It was evident that many large cracks were developed in confined concrete in both of the specimens. The number of cracks and the length of the crack-forming zone were higher for the GFRP strengthened specimen than the CFRP wrapped one. This might be due to the additional hoop layer in the CFRP wrapped specimen.

4.2 FRP orientation

The unidirectional FRP laminates are mainly strong along the length of the fibres. Thus, the effect of the orientation of fibre direction has been investigated by considering different FRP orientations in the strengthening scheme. The comparison of lateral displacement responses of one, two and three layers wrapped specimens with seven different FRP orientations were examined, as shown in Fig. 13(a). One layer strengthened specimens in longitudinal and hoop directions exhibited nearly similar peak lateral displacements. But, the residual lateral displacement of the specimen orientated in a longitudinal direction was 13% higher than that of the hoop-orientated specimen. In the case of two layers FRP wrapped specimens, only the longitudinal orientation of FRP demonstrated superior performance by controlling global deformation compared to the combination of hoop and longitudinal layers (Fig. 13(a)). However, including a hoop layer into the CFRP wrapping scheme was effective to minimise peak lateral displacement from 74.4 mm (CCFT-LLL-V1) to 72.7 mm (CCFT-LHL-V1), as listed in Table 3. This might be due to the composite action of the longitudinal-hoop-longitudinal orientation, which provided better confinement in both hoop and longitudinal directions. It can be seen from the failure modes (Fig. 14) of FRP wrapped specimens that the three layers longitudinally wrapped specimen (CCFT-LLL-V1) showed large debonding at the side of the specimen. CFRP damage and breakage failures were found at both tension and compression faces of the specimen. The one layer and two layers longitudinally wrapped specimens also experienced severe debonding and fibre breakage failure (Figs. 11 and 14). It was observed from the high-speed camera during the test that after the initiation of CFRP breakage failure at the bottom of the longitudinally wrapped specimens, the CFRP laminates started separating from the steel surfaces due to the absence of a hoop layer. However, introducing hoop layers into the wrapping orientation effectively controlled such kind of debonding failure as shown in Figs. 11 and 14. The common failure modes of the combined

longitudinal and hoop layer were fibre breakage at the tension face and fibre damage and breakage at the compression face of the specimens. The advantages of hoop orientation to enhance structural performance of CHS beams under static bending loading have also been reported in early studies [14, 17].

4.3 FRP thickness

The influence of CFRP confining thickness has been examined by varying CFRP layers of the strengthened specimens. The peak lateral displacement was maximum for the CCFT-L-V1 member (Fig. 12(a)). The reduction of peak lateral displacement can be achieved up to 11% by three layers of CFRP wrapping (CCFT-LHL-V1). Thus, increasing CFRP thickness is beneficial to control the lateral deflection of the CFST specimens. It can be seen that increasing the CFRP layer in only a longitudinal direction could not help to prevent debonding failure of the CFRP laminates, as shown in Fig. 15. The severity of debonding failure increased with the increase of longitudinally wrapped CFRP layers (Fig. 15). The additional self-weight and increased flexure stiffness of thicker (two and three layers) CFRP laminates might contribute to the extension of debonded CFRP laminates. Thus, fracture and debonding of CFRP laminates were more prominent in specimens with two and three layers of CFRP wrapping. However, the composite action of longitudinal and hoop layers effectively eliminated the debonding failure tendency of longitudinally wrapped CFRP laminates (Fig. 15). Therefore, it is highly important to select the appropriate CFRP orientation scheme for better control of lateral deflection and debonding failure of CFRP laminates due to the lateral impact.

4.4 bond length

The bond length of CFRP laminates varied to investigate the effect of changing CFRP wrapping lengths on the responses of CFST specimens under lateral impact. Four two layers

longitudinally wrapped specimens with bond length of 1300 mm (full bond length), 1080 mm, 865 mm and 650 mm were considered in this study. Fig. 16 shows the lateral displacement-time graphs of bare and strengthened specimens with various bond lengths. The peak lateral displacement of bare specimens reduced from 87 mm to 84.5 mm due to the strengthening of half bond length (650 mm). However, no noticeable change of residual lateral displacements was found. The reason behind this might be the debonding phenomena of CFRP laminates in longitudinally wrapped specimens. Further increase of bond length to 865 mm also depicted a little enhancement of stiffness of the strengthened member as the reduction of peak and residual displacements was not noticeable. The maximum lateral displacement reduced from 79.3 mm to 76.5 mm with a bond length from 1080 mm to full bond length. Thus, this research did not find any reduced effective bond length, as with the increase of wrapping length, lateral displacement of the specimens also reduced as shown in Fig. 17. This may be due to the debonding tendency of CFRP at reduced bond length. Large debonding, severe CFRP breakage and fracture and complete separation of CFRP laminates were observed for the specimens with different bond lengths (Fig. 14). This is obvious, as similar CFRP failure patterns were also observed in full-length wrapped member (CCFT-LL-V1) (Fig. 14). The poor bonding performance of only longitudinally wrapped members might be the key cause of these kinds of failure. The combination of longitudinal and hoop layers can be the alternative to avoid debonding failures of the CFRP wrapped specimens.

4.5 Impact velocity

The initial impact velocities of 5 m/s and 3.28 m/s were selected to observe the effects of velocity changes of two layers CFRP wrapped specimens in a longitudinal direction. A considerable reduction of lateral displacements was observed for both bare and wrapped specimens, as shown in Fig. 8. The reductions of peak displacements were calculated as 12% and 24% for 5 m/s and 3.28 m/s impact velocities, respectively. The residual lateral

displacements were reduced by21% and 35%, when subjected to 5 m/s and 3.28 m/s impact velocities, respectively. Thus, CFRP wrapping was more effective in low impact velocity than the higher impact velocity. This can be explained as with the increase of impact velocity or impact energy, the severity of CFRP laminate failure also increased, hence effectiveness of CFRP wrapping was reduced. Fig. 18 shows the impact force time-history comparison of bare and strengthened specimens. The impact force-time curves indicate that with the increase of impact velocity, the peak initial impact force also increased (Fig. 18). Interestingly, the contact durations between the specimens and the impact hammer were shorter for wrapped members compared to their bare counterparts. This is due to the increased stiffness of the wrapped members. Because of the higher stiffness, the impact hammer rebounded more quickly from the strengthened members than the corresponding bare members. Typical global deformation failure was noticed for the bare specimen whereas fibre breakage and debonding failures were observed in the tension face of the wrapped specimen (Fig. 14). This confirms that CFRP laminates in only a longitudinal direction are highly prone to lateral impact loading even in lower impact velocity.

5. Comparison with early studies

A comparison of the percentage of reduction of lateral displacements between the current experimental results and recent experimental tests [37, 38] of FRP strengthened CFST members subjected to drop hammer impact, is presented in Fig. 19. The reduction percentages were calculated by dividing the peak lateral displacements by their corresponding values for bare specimens. The effect of support conditions, impactor shape and span length of the specimens were not considered in this comparison study. It can be seen that the lateral displacement control ability of the specimens from Chen et al. [37] tests was much more higher than the wrapped specimens in the current study and Shakir et al. [38].

However, Chen et al. [37] experimental impact tests showed only elastic deformations, as specimens reached zero deflection at the end of impact tests. The actual contribution of FRP strengthening could be more understandable if the specimens experienced plastic deformation for utilising the capacity of the bonded FRP against lateral impact. In the case of Shakir et al. [38] tests, FRP strengthening mainly helped to reduce lateral displacements of plastically deformed CFST specimens filled with recycled aggregates (RA) (Fig. 19) and was not effective for normal concrete. The results of the current experimental investigation indicated that, the FRP strengthening effectively reduced (a maximum of 18% residual displacement reduction was observed) the lateral displacement of plastically deformed CFST members subjected to transverse impact. However, strength enhancement of CFRP strengthened specimens might not be as prominent as specimens under static loading due to the debonding tendency of CFRP laminates under dynamic impact. Utilisation of GFRP laminates can be an alternative to achieve better impact resistance and prevent debonding failure because of superior toughness properties of GFRP laminates under lateral impact loading. However, more research should carry out to improve the bond behaviour between CFRP and steel members under lateral impact loading to fully utilise the capacity of CFRP laminates.

6. Conclusions

In this paper, drop hammer impact tests of FRP strengthened CFST specimens were carried out to understand the structural responses and failure modes of CFST members under lateral impact. The test results and observations of this experimental study can be summarised as below:

- High initial peak impact forces were observed for all the tested specimens. A maximum of 21.3% variation of peak impact forces were estimated due to the difference of contact surface hardness. No significant changes in residual forces were

noticed. The residual lateral displacement of the bare CFST member can be reduced up to 18% by strengthening with three layers CFRP sheets.

- The global deformation of CFST members was the common failure mode observed for all the specimens. Externally bonded CFRP sheets seemed to be highly prone to local failure due to lateral impact in both compression and tension faces of impact location. CFRP breakage, debonding, cracking and fibre damages were the typical failure modes of CFRP laminates found after the impact tests. The prominent cracks and separation of core concrete were noticed in the bare member. However, CFRP wrapping helped to minimise the cracks' width and prevent separation of core concrete.
- Compared to CFRP laminates, GFRP laminates provided superior performance for CFST members by minimising both peak and residual displacements. CFRP sheets exhibited severe fibre breakage and debonding failure. Introducing only GFRP layers and a combined GFRP and CFRP layer into the wrapping system can effectively minimise the CFRP laminate failures.
- An appropriate CFRP orientation system should be adopted to expect better enhancement in impact performance due to CFRP strengthening of CFST members. While longitudinal FRP layers are key contributors to control global deflection by carrying additional loads from tension face, at the same time, such layers have a high tendency for debonding failure due to the absence of hoop layers. Therefore, it is highly recommended to include one hoop layer in the wrapping scheme to minimise CFRP debonding under impact loading.
- The thickness of CFRP wrapping played a key role in deflection control of CFST members. One layer, two layers and three layers CFRP wrapped specimens minimised 6.7%, 12% and 16.4% of peak lateral displacements of bare specimen, respectively.

Due to the severe debonding phenomena of longitudinally wrapped specimens, effective bond length could not be estimated for this study. It is recommended to include a hoop layer for investigating the effect of bond length in any future research.

- The effect of initial impact velocity is noticeable as with the reduction of velocity from 5 m/s to 3.28 m/s, the percentage of residual displacement reduction increased from 21% to 35%. However, CFRP strengthened members in longitudinal directions exhibited debonding failure, even though initial impact velocity reduced from 5 m/s to 3.28 m/s. The comparison of present work with a number of recent studies has shown that with the reduction of impact energy, the efficiency of CFRP to control lateral impact increased remarkably. It was also found that GFRP laminates proved to be a better strengthening option than CFRP laminates under lateral impact loading because its superior toughness performance.

It should be noted that appropriate surface preparation and selection of suitable FRP and adhesives are important in applying this technique. Based on the current impact test results, it is found that FRP strengthening of CFST members can be implemented to minimise the damage and failure of such members under transverse impact. However, further research with full-scale specimens and more realistic impact loading will aid to the design guidelines and cost-effective field application of this technique.

Acknowledgement

The authors would like to thank technical staffs, Mr. Alan Grant, Mr. Cameron Neilson and Mr. Travis Marshall for their assistance in the experimental work at University of Wollongong laboratory. The authors would also like to thank Queensland University of Technology (QUT) and Tsinghua Initiative Scientific Research Program (No. 20131089347) for providing support to carry out the work reported in this paper.

References

[1] Han L-H, Li W, Bjorhovde R. Developments and advanced applications of concrete-filled steel tubular (CFST) structures: Members. Journal of Constructional Steel Research. 2014;100:211-28.

[2] Fawzia S, Zhao X, Al-Mahaidi R, Rizkalla S. Bond characteristics between CFRP and steel plates in double strap joints. The International Journal of Advanced Steel Construction. 2005;1:17-27.

[3] Fawzia S, Al-Mahaidi R, Zhao X-L. Experimental and finite element analysis of a double strap joint between steel plates and normal modulus CFRP. Composite structures. 2006;75:156-62.

[4] Fawzia S, Zhao X-L, Al-Mahaidi R. Bond–slip models for double strap joints strengthened by CFRP. Composite Structures. 2010;92:2137-45.

[5] Fawzia S. Evaluation of shear stress and slip relationship of composite lap joints. Composite Structures. 2013;100:548-53.

[6] Al-Zubaidy H, Al-Mahaidi R, Zhao X-L. Experimental investigation of bond characteristics between CFRP fabrics and steel plate joints under impact tensile loads. Composite Structures. 2012;94:510-8.

[7] Batuwitage C, Fawzia S, Thambiratnam D, Al-Mahaidi R. Durability of CFRP strengthened steel plate double-strap joints in accelerated corrosion environments. Composite Structures. 2016 (In press).

[8] Al-Zubaidy H, Zhao X-L, Al-Mahaidi R. Mechanical characterisation of the dynamic tensile properties of CFRP sheet and adhesive at medium strain rates. Composite Structures. 2012;96:153–64.

[9] Al-Mosawe A, Al-Mahaidi R, Zhao X-L. Bond behaviour between CFRP laminates and steel members under different loading rates. Composite Structures. 2016;148:236-51.

[10] Al-Mosawe A, Al-Mahaidi R, Zhao X-L. Experimental and Numerical Study on Strengthening of Steel Members Subjected to Impact Loading Using Ultrahigh Modulus CFRP. Journal of Composites for Construction. 2016;0:04016044.

[11] Shaat A, Fam A. Axial loading tests on short and long hollow structural steel columns retrofitted using carbon fibre reinforced polymers. Canadian Journal of Civil Engineering. 2006;33:458-70.

[12] Shaat A, Fam A. Slender Steel Columns Strengthened Using High-Modulus CFRP Plates for Buckling Control. Journal of Composites for Construction. 2009;13:2-12.

[13] Fawzia S, Al-Mahaidi R, Zhao X, Rizkalla S. Strengthening of circular hollow steel tubular sections using high modulus CFRP sheets. Construction and Building Materials. 2007;21:839-45.

[14] Haedir J, Bambach M, Zhao X-L, Grzebieta R. Strength of circular hollow sections (CHS) tubular beams externally reinforced by carbon FRP sheets in pure bending. Thin-Walled Structures. 2009;47:1136-47.

[15] Haedir J, Zhao X-L. Design of short CFRP-reinforced steel tubular columns. Journal of Constructional Steel Research. 2011;67:497-509.

[16] Gao X, Balendra T, Koh C. Buckling strength of slender circular tubular steel braces strengthened by CFRP. Engineering Structures. 2013;46:547-56.

[17] Kabir MH, Fawzia S, Chan THT, Gamage JCPH, Bai JB. Experimental and numerical investigation of the behaviour of CFRP strengthened CHS beams subjected to bending. Engineering Structures. 2016;113:160-73.
[18] Kabir MH, Fawzia S, Chan THT, Gamage JCPH. Comparative durability study of CFRP strengthened tubular steel members under cold weather. Materials and Structures. 2016;49:1761-74.
[19] Kabir MH, Fawzia S, Chan THT. Durability of CFRP strengthened circular hollow steel members under cold weather: Experimental and numerical investigation. Construction and Building Materials. 2016;123:372-83.
[20] Kabir MH, Fawzia S, Chan THT, Badawi M. Numerical studies on CFRP strengthened steel circular members under marine environment. Materials and Structures. 2016:1-16.
[21] Kabir MH, Fawzia S, Chan THT, Badawi M. Durability of CFRP strengthened steel circular hollow section member exposed to sea water. Construction and Building Materials. 2016;118:216-25.
[22] Alam MI, Fawzia S. Numerical studies on CFRP strengthened steel columns under transverse impact. Composite Structures. 2015;120:428-41.
[23] Alam MI, Fawzia S, Liu X, Batuwitage C. Dynamic simulation of CFRP strengthened steel column under impact loading. In: proceedings of 23rd Australasian Conference on the Mechanics of Structures and Materials (ACMSM23). Byron Bay, Australia; 2014. p. 503-08.
[24] Alam MI, Fawzia S, Zhao X-L, Remennikov A. Experimental Study on FRP-Strengthened Steel Tubular Members under Lateral Impact. Journal of Composites for Construction. 2017; DOI: http://dx.doi.org/10.1061/(ASCE)CC.1943-5614.0000801 .
[25] Xiao Y. Applications of FRP composites in concrete columns. Advances in Structural Engineering. 2004;7:335-43.
[26] Xiao Y, He W, Choi K-k. Confined concrete-filled tubular columns. Journal of structural engineering. 2005;131:488-97.
[27] Tao Z, Han L-H, Zhuang J-P. Axial loading behavior of CFRP strengthened concrete-filled steel tubular stub columns. Advances in Structural Engineering. 2007;10:37-46.
[28] Hu Y, Yu T, Teng J. FRP-confined circular concrete-filled thin steel tubes under axial compression. Journal of Composites for Construction. 2011;15:850-60.
[29] Vincent T, Ozbakkaloglu T. Influence of concrete strength and confinement method on axial compressive behavior of FRP confined high- and ultra high-strength concrete. Composites Part B: Engineering. 2013;50:413-28.
[30] Abdalla S, Abed F, AlHamaydeh M. Behavior of CFSTs and CCFSTs under quasi-static axial compression. Journal of Constructional Steel Research. 2013;90:235-44.
[31] Ganesh Prabhu G, Sundarraja MC, Kim YY. Compressive behavior of circular CFST columns externally reinforced using CFRp composites. Thin-Walled Structures. 2015;87:139-48.
[32] Dong JF, Wang QY, Guan ZW. Structural behaviour of recycled aggregate concrete filled steel tube columns strengthened by CFRP. Engineering Structures. 2013;48:532-42.
[33] Remennikov A, Kong S, Uy B. Response of Foam- and Concrete-Filled Square Steel Tubes under Low-Velocity Impact Loading. Journal of Performance of Constructed Facilities. 2011;25:373-81.

[34] Yousuf M, Uy B, Tao Z, Remennikov A, Liew JYR. Impact behaviour of pre-compressed hollow and concrete filled mild and stainless steel columns. Journal of Constructional Steel Research. 2014;96:54-68.
[35] Han L-H, Hou C-C, Zhao X-L, Rasmussen KJ. Behaviour of high-strength concrete filled steel tubes under transverse impact loading. Journal of Constructional Steel Research. 2014;92:25-39.
[36] Wang R, Han L-H, Hou C-C. Behavior of concrete filled steel tubular (CFST) members under lateral impact: Experiment and FEA model. Journal of Constructional Steel Research. 2013;80:188-201.
[37] Chen C, Zhao Y, Li J. Experimental investigation on the impact performance of concrete-filled FRP steel tubes. Journal of Engineering Mechanics. 2014;0:04014112.
[38] Shakir AS, Guan ZW, Jones SW. Lateral impact response of the concrete filled steel tube columns with and without CFRP strengthening. Engineering Structures. 2016;116:148-62.
[39] Alam MI, Fawzia S, Liu X. Effect of bond length on the behaviour of CFRP strengthened concrete-filled steel tubes under transverse impact. Composite Structures. 2015;132:898-914.
[40] Alam MI, Fawzia S, Zhao X-L. Numerical investigation of CFRP strengthened full scale CFST columns subjected to vehicular impact. Engineering Structures. 2016;126:292-310.
[41] Alam MI, Fawzia S, Batuwitage C. CFRP strengthened CFST columns under vehicular impact. Proceedings of the Second International Conference on Performance-based and Life-cycle Structural Engineering: University Of Queensland & The Hong Kong Polytechnic University; 2015. p. 459-65.
[42] AS1012.9. Methods of testing concrete-determination of the compressive strength of concrete specimens. Sydney, Australia: Standards Australia; 1999.
[43] AS1012.8.2. Method for making and curing concrete-Flexure test specimens. Sydney, Australia: Standards Australia; 2014.
[44] AS/NZS1163. Cold-formed structural steel hollow sections. Standard Australia. Sydney, Australia.: Standard Australia; 2009.
[45] AS1391. Metallic mateials–tensile testing at ambient temperature. Sydney, Australia: Standard Australia; 2007.
[46] ASTM:D3039. Standard Test Method for Tensile Properties of Polymer Matrix Composite Materials. West Conshohocken, PA, USA: ASTM International; 2008.
[47] Jiao H, Zhao XL. CFRP strengthened butt-welded very high strength (VHS) circular steel tubes. Thin-Walled Structures. 2004;42:963-78.
[48] Fernando D, Teng J, Yu T, Zhao X. Preparation and Characterization of Steel Surfaces for Adhesive Bonding. Journal of Composites for Construction. 2013;17:04013012.
[49] Schnerch D, Dawood M, Rizkalla S, Sumner E. Proposed design guidelines for strengthening of steel bridges with FRP materials. Construction and Building Materials. 2007;21:1001-10.
[50] Goldston M, Remennikov A, Sheikh MN. Experimental investigation of the behaviour of concrete beams reinforced with GFRP bars under static and impact loading. Engineering Structures. 2016;113:220-32.

[51] Tao Z, Han L-H, Wang L-L. Compressive and flexural behaviour of CFRP-repaired concrete-filled steel tubes after exposure to fire. Journal of Constructional Steel Research. 2007;63:1116-26.
[52] Bambach M. Design of hollow and concrete filled steel and stainless steel tubular columns for transverse impact loads. Thin-Walled Structures. 2011;49:1251-60.

Figure Captions:

Fig. 1.	Concrete (a) uniaxial compression, (b) four point flexure test setup.
Fig. 2.	Tensile coupon tests of CFRP laminate (left) and GFRP laminate (right).
Fig. 3.	Preparation of test specimens.
Fig. 4.	(a) Test set up (schematic view), (b) drop hammer impact facility with test specimen.
Fig. 5.	Impact force-time curves of bare and CFRP strengthened specimens.
Fig. 6.	(a) Lateral displacement time histories obtained from laser sensor and video frames, (b) initiation of CFRP breakage and debonding.
Fig. 7.	Validation of displacement time curves obtained from high-speed video frames.
Fig. 8.	Lateral displacement-time history comparison of bare and CFRP strengthened specimens.
Fig. 9.	Impact force -lateral displacement curves of test specimens.
Fig. 10.	Failure progress of bare and CFRP strengthened specimens obtained from high-speed camera frames.
Fig. 11.	Failure modes of bare and CFRP strengthened CFST members after lateral impact.
Fig. 12.	Failure mode of core concrete at tension face of the specimens.
Fig. 13.	(a) Lateral displacement versus time graphs of FRP wrapped specimens with different FRP types, FRP orientations, and FRP thicknesses, (b) impact force-lateral displacement curves of CFRP and GFRP wrapped specimens.
Fig. 14.	Failure modes of strengthened members.
Fig. 15.	Failure mode comparison of specimens with various CFRP thicknesses.
Fig. 16.	Effect of CFRP bond length.
Fig. 17.	Maximum lateral displacement-bond length relationships of CFRP strengthened specimens.
Fig. 18.	Effects of initial impact velocity on impact force-time responses.
Fig. 19.	Comparison of lateral displacement reduction of FRP laminates.

List of Figures:

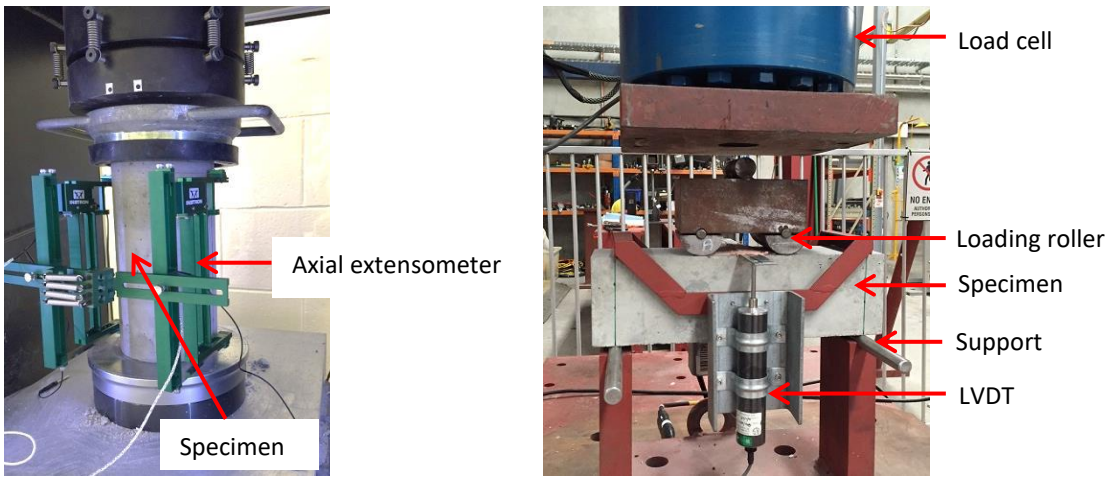

(a) (b)

Fig. 1. Concrete (a) uniaxial compression, (b) four point flexure test setup.

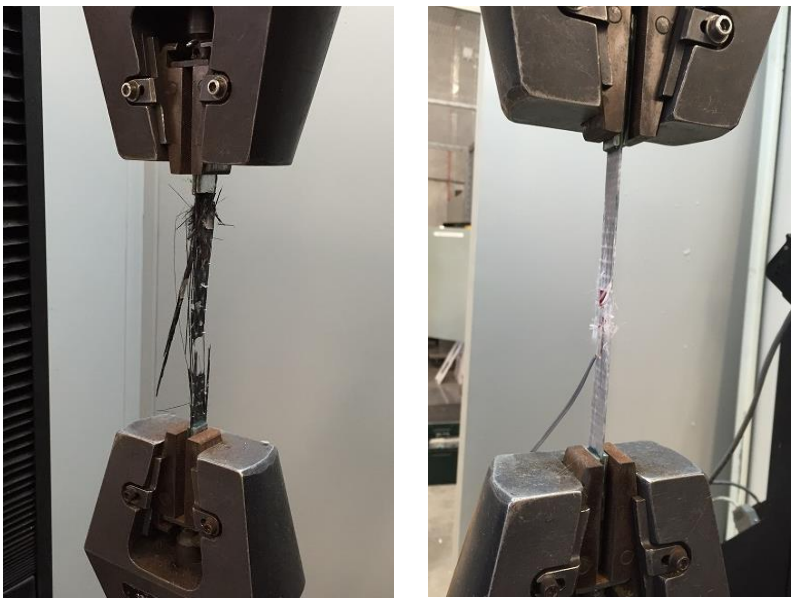

Fig. 2. Tensile coupon tests of CFRP laminate (left) and GFRP laminate (right).

(a) specimens after surface preparation

(b) FRP strengthened specimens

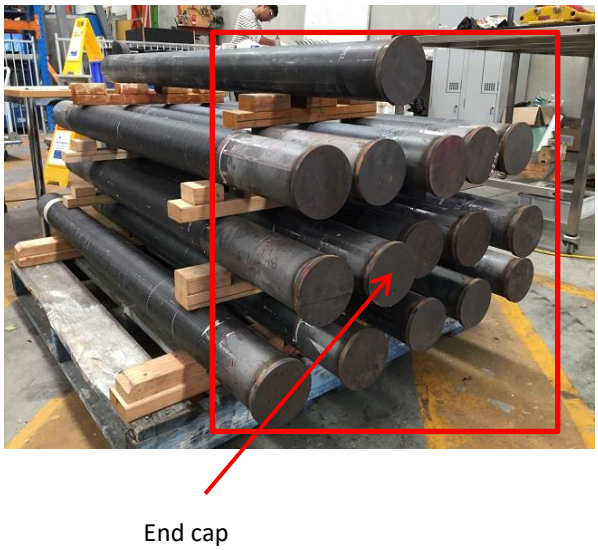

(c) FRP strengthened specimens with end cap

(d) concrete filling of specimens

Fig. 3. Preparation of test specimens.

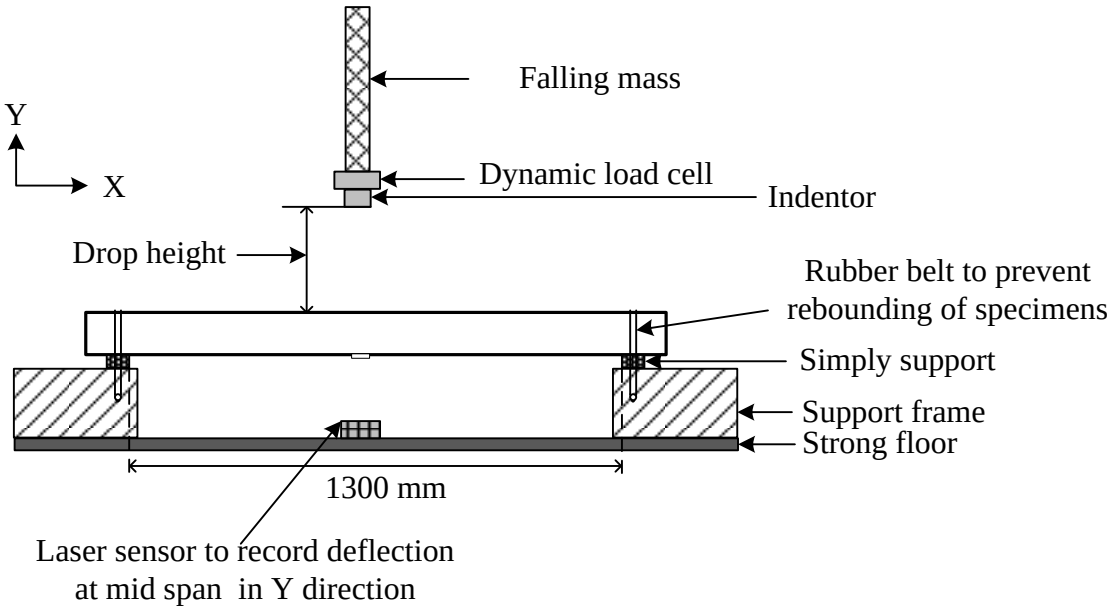

(a)

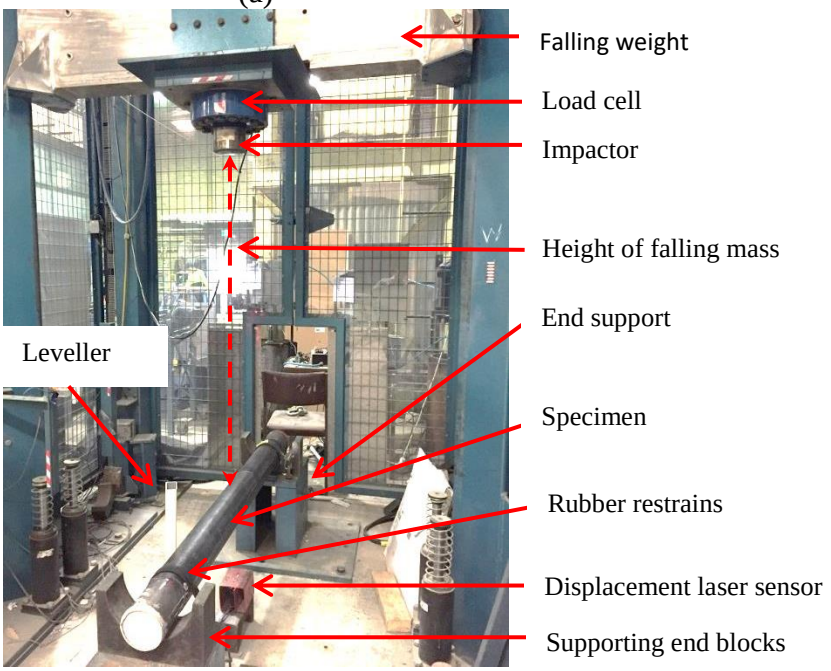

(b)

Fig. 4. (a) Test setup (schematic view), (b) drop hammer impact facility with test specimen.

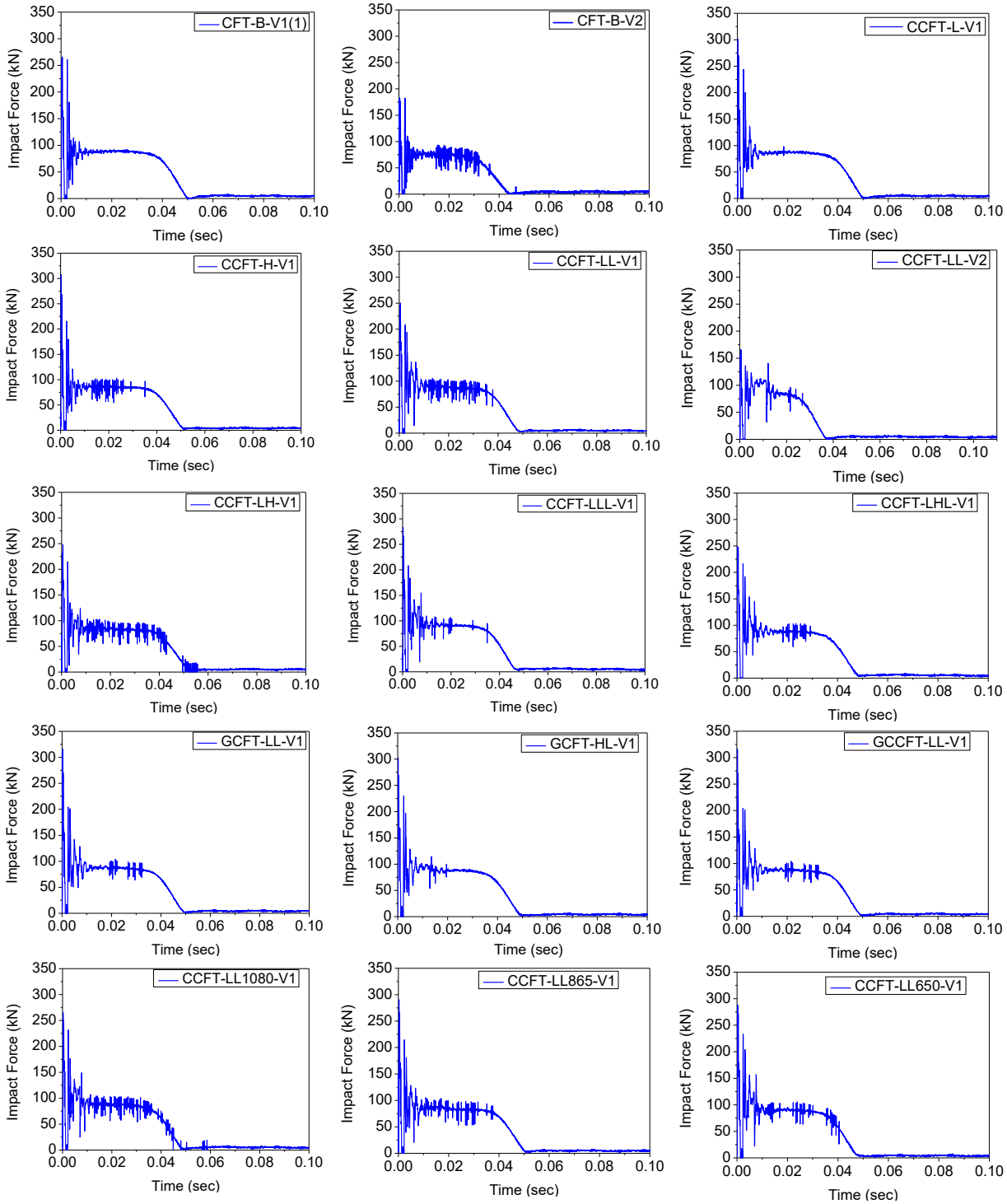

Fig. 5. Impact force-time curves of bare and CFRP strengthened specimens.

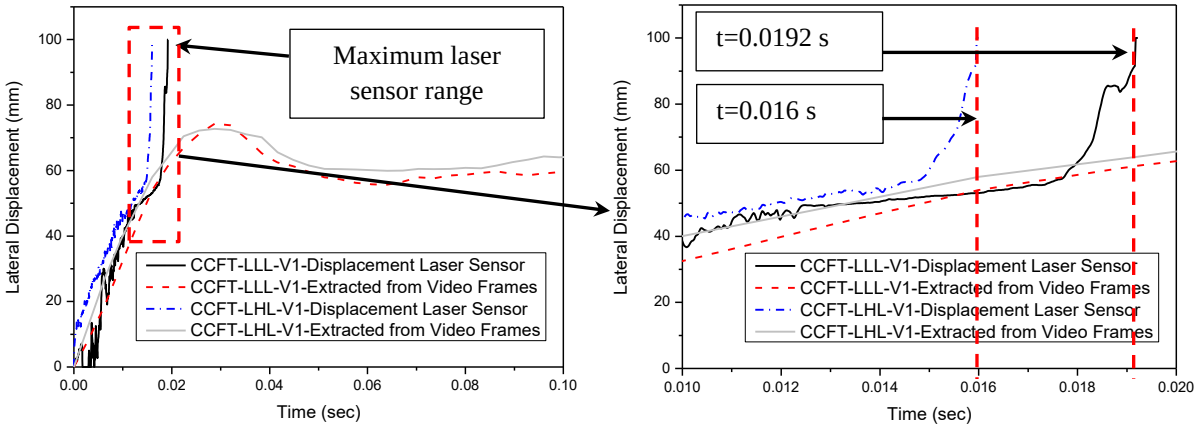

(a)

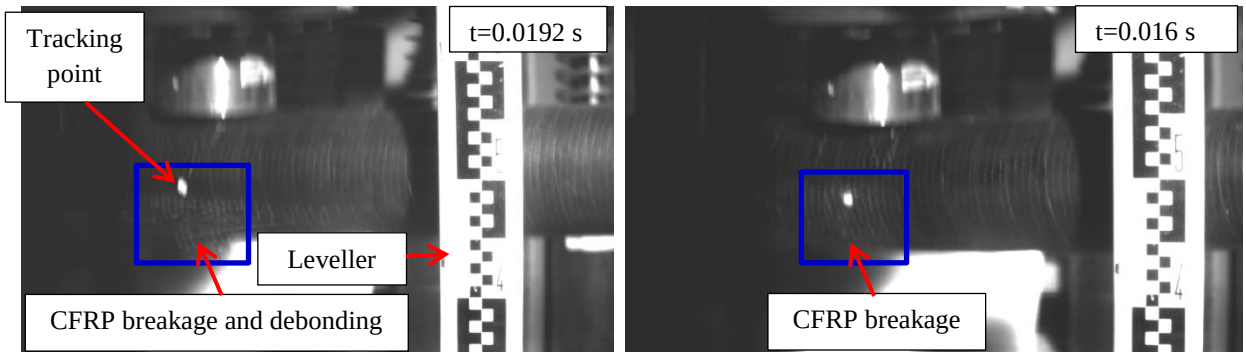

CCFT-LLL-V1 CCFT-LHL-V1

(b)

Fig. 6. (a) Lateral displacement time histories obtained from laser sensor and video frames, (b) initiation of CFRP breakage and debonding.

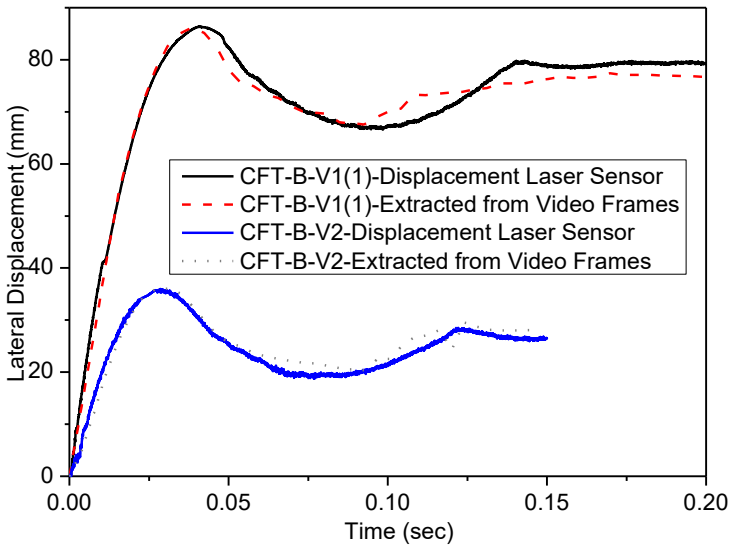

Fig. 7. Validation of displacement time curves obtained from high-speed video frames.

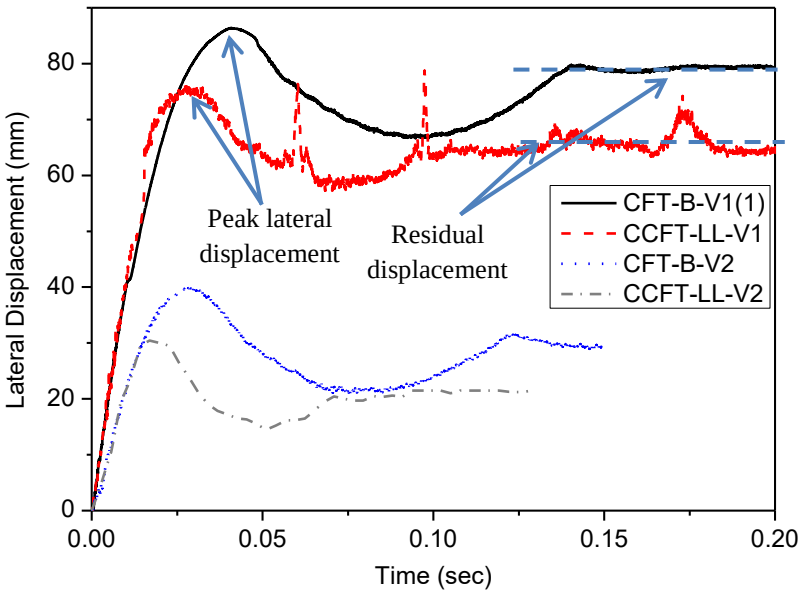

Fig. 8. Lateral displacement-time history comparison of bare and CFRP strengthened specimens.

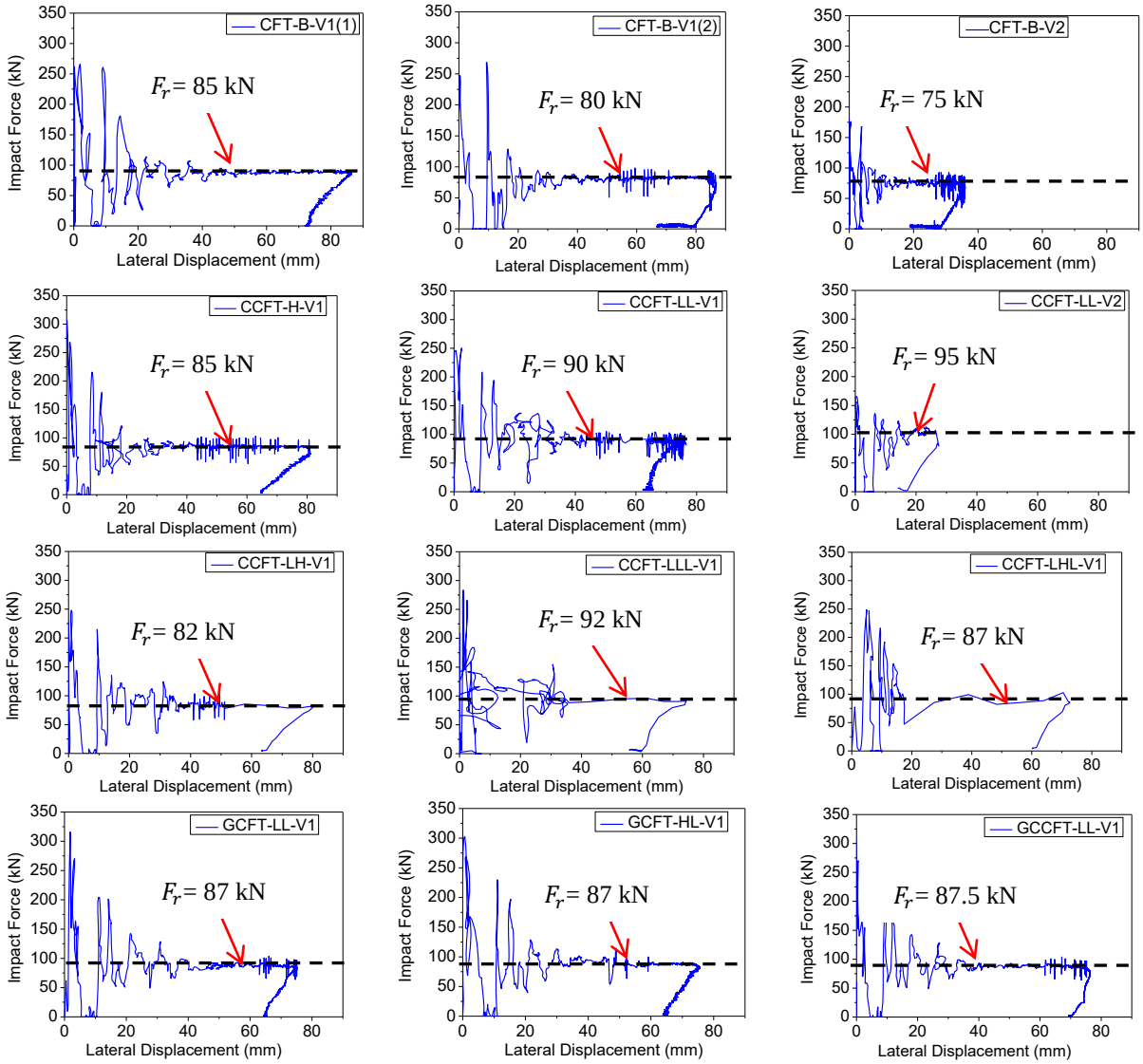

Fig. 9. Impact force -lateral displacement curves of test specimens.

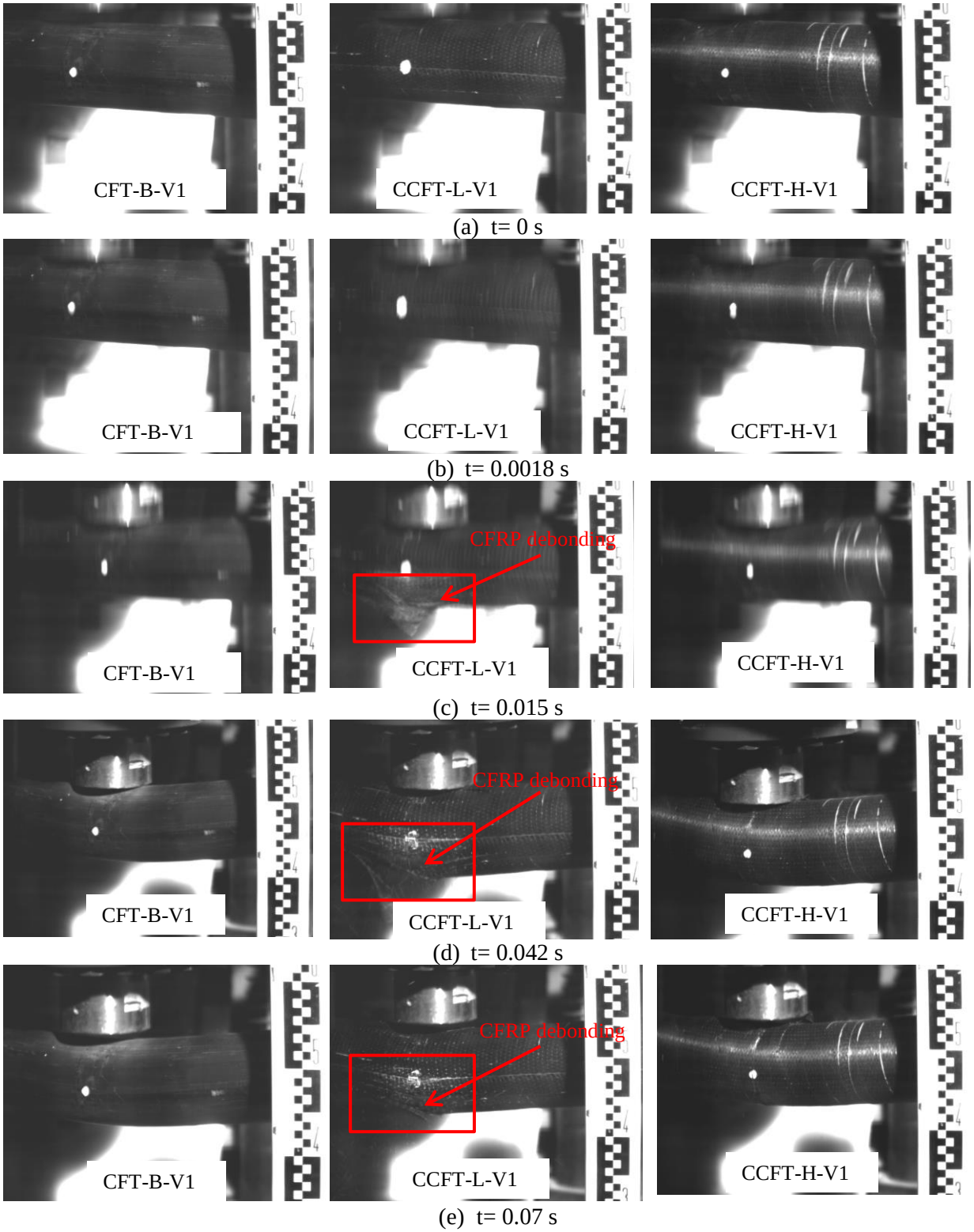

Fig. 10. Failure progress of bare and CFRP strengthened specimens obtained from high-speed camera frames.

CFT-B-V1

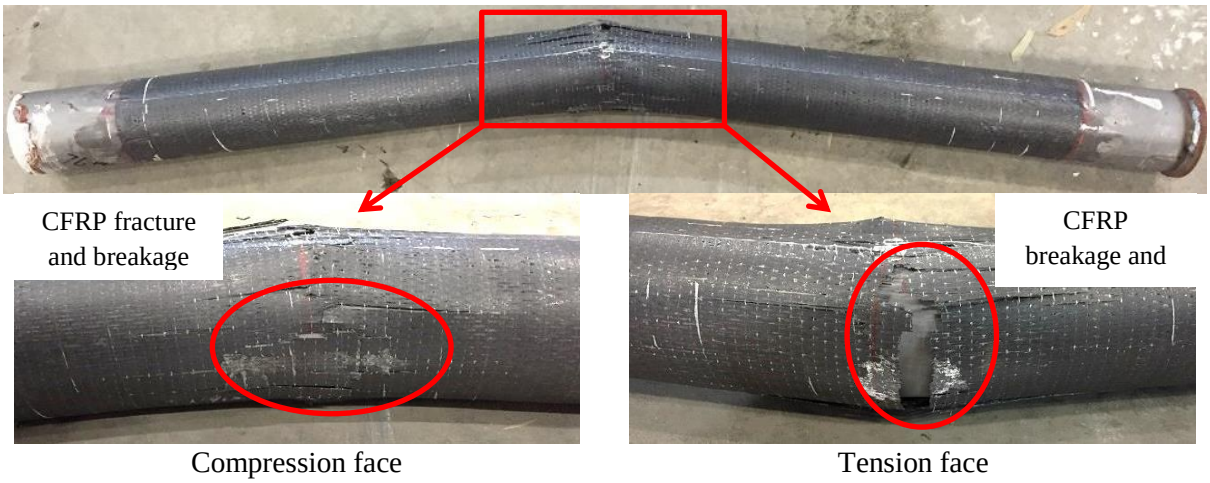

CCFT-L-V1

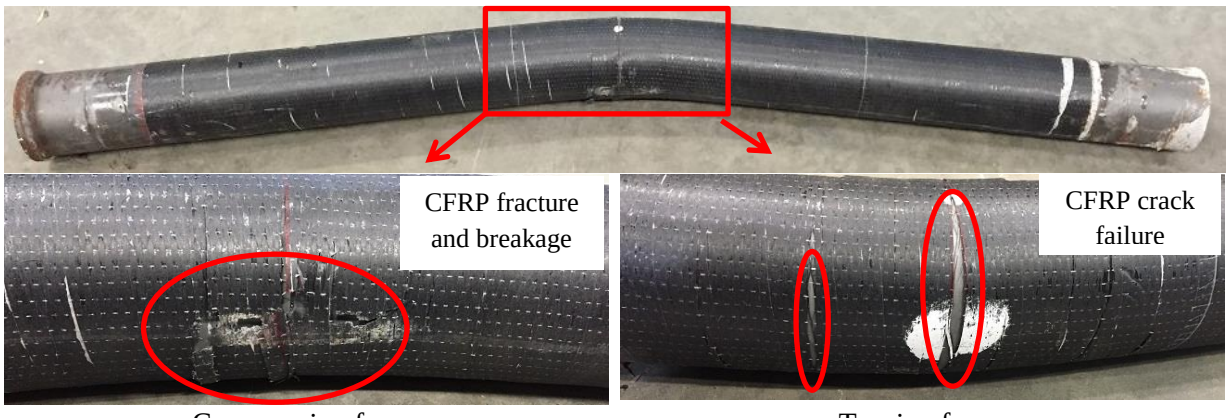

CCFT-H-V1

Fig. 11. Failure modes of bare and CFRP strengthened CFST members after lateral impact.

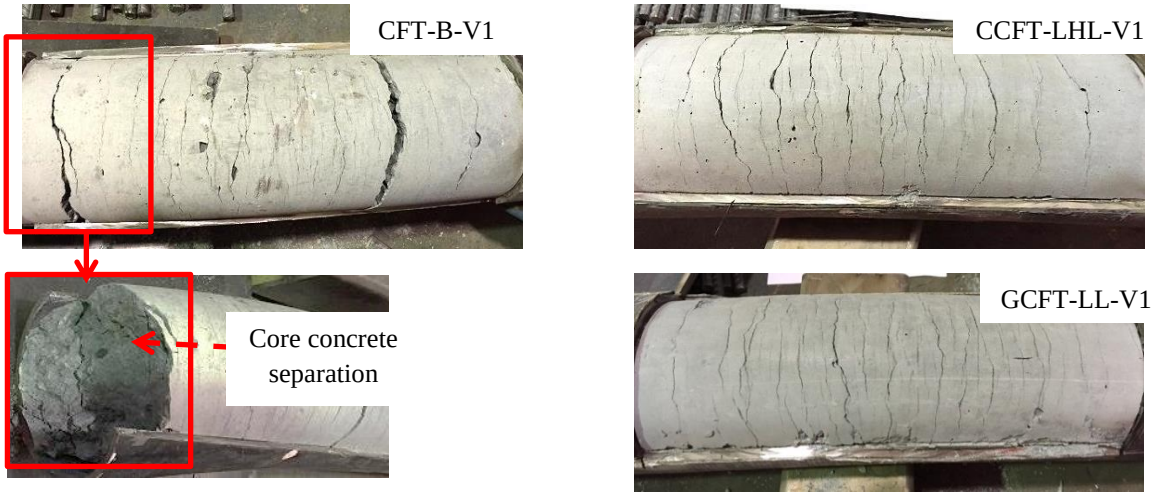

Fig. 12. Failure mode of core concrete at tension face of the specimens.

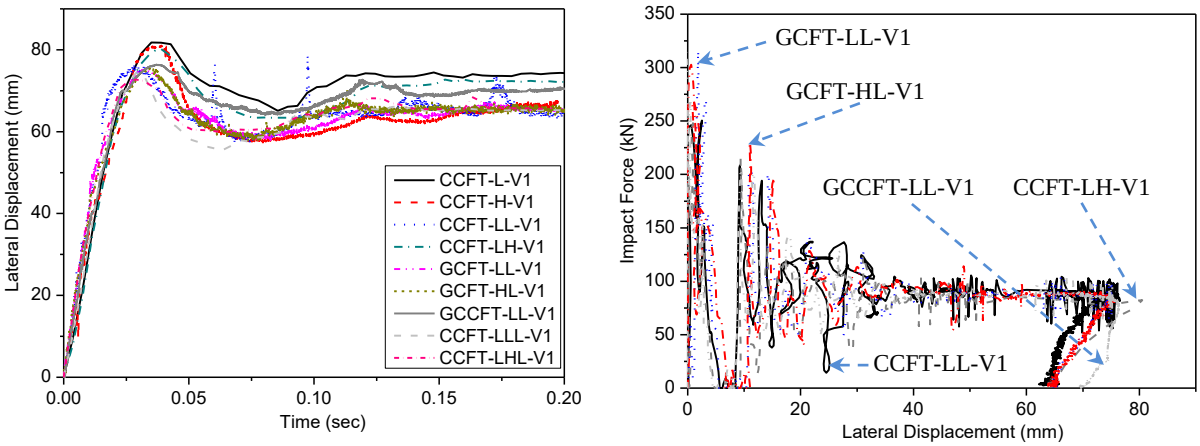

(a) (b)

Fig. 13. (a) Lateral displacement versus time graphs of FRP wrapped specimens with different FRP types, FRP orientations, and FRP thicknesses, (b) impact force-lateral displacement curves of CFRP and GFRP wrapped specimens.

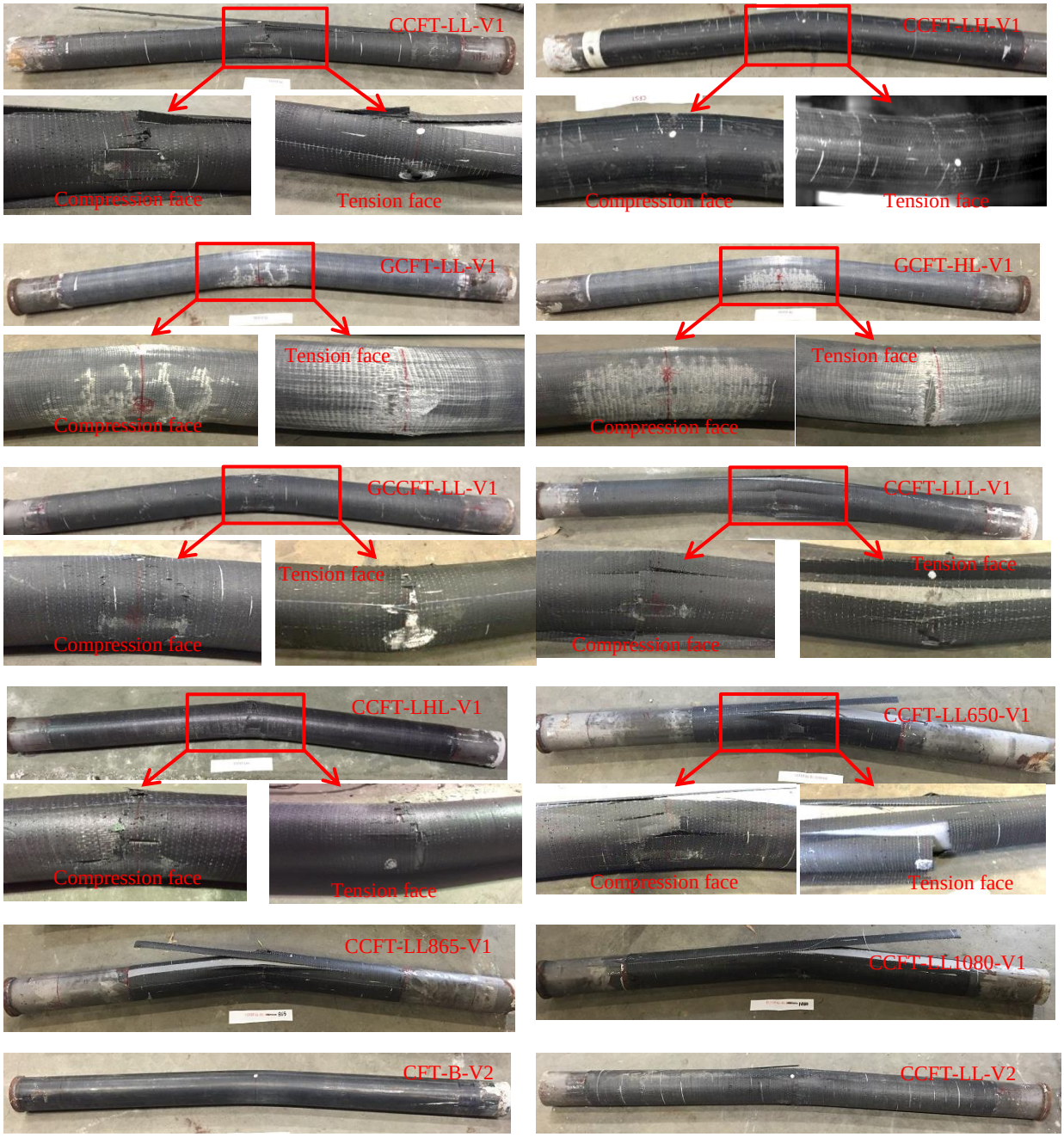

Fig. 14. Failure modes of strengthened members.

Fig. 15. Failure mode comparison of specimens with various CFRP thicknesses.

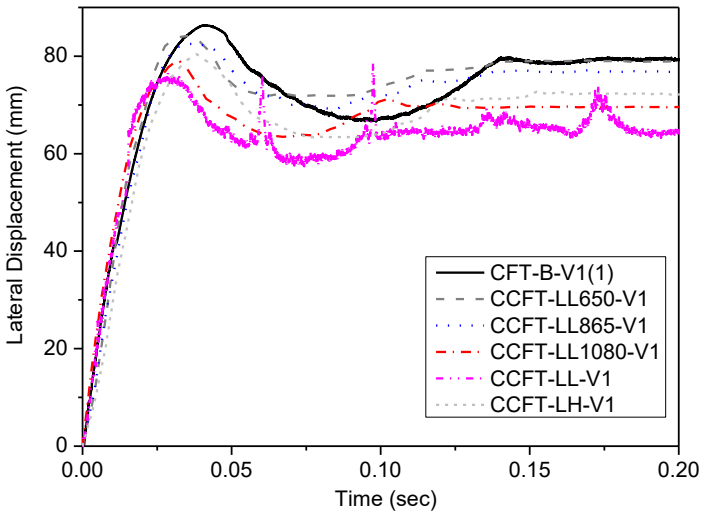

Fig. 16. Effect of CFRP bond length.

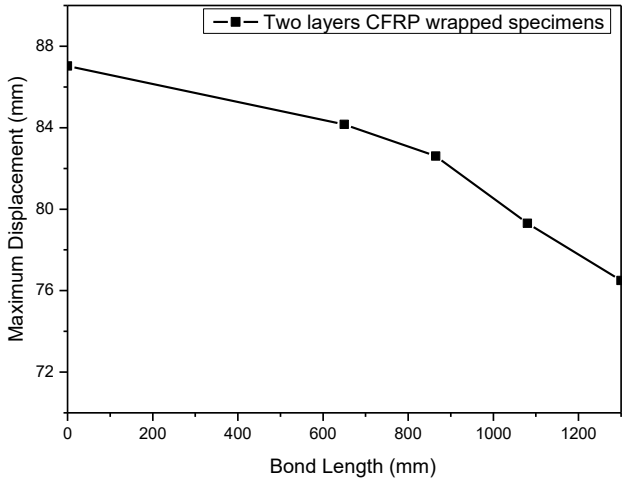

Fig. 17. Maximum lateral displacement-bond length relationships of CFRP strengthened specimens.

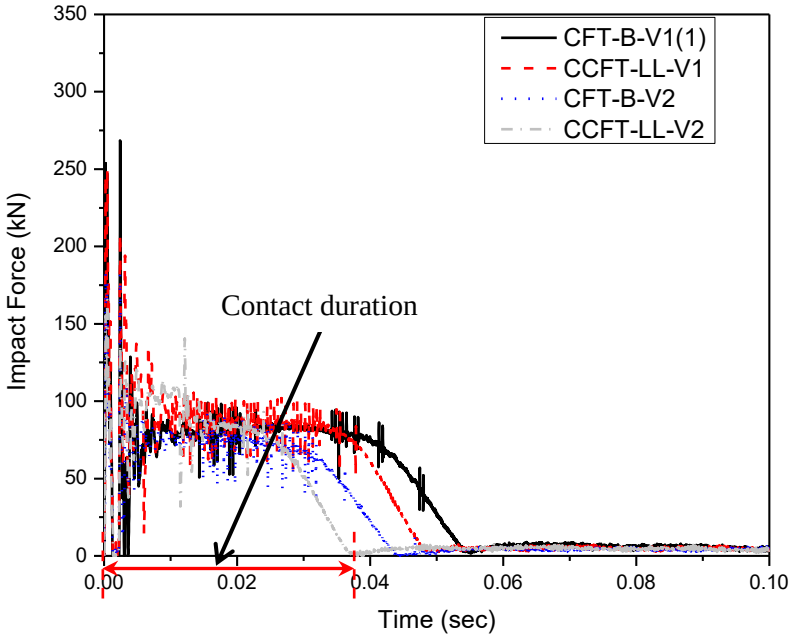

Fig. 18. Effects of initial impact velocity on impact force-time responses.

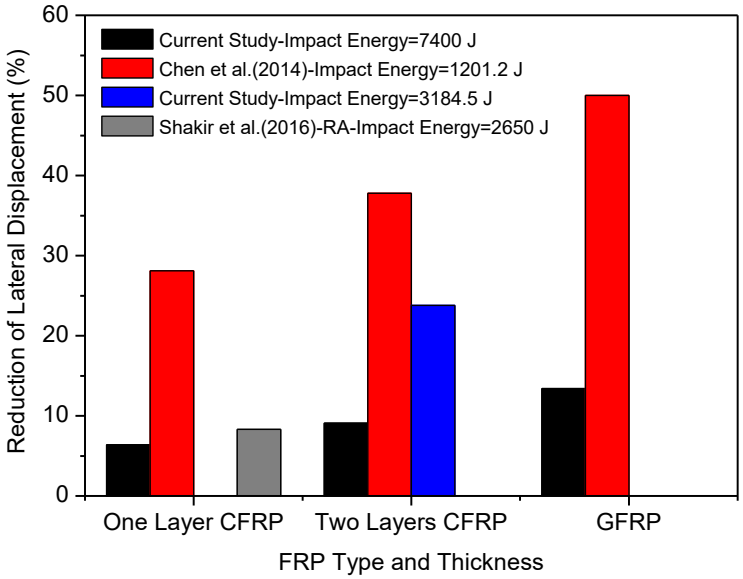

Fig. 19. Comparison of lateral displacement reduction of FRP laminates.

List of Tables:

Table 1	Mechanical properties of materials used for specimen preparation
Table 2	Details of impact test specimens
Table 3	Impact test results
Table 4	Absorption of impact energy due to global deformation

Table 1. Mechanical properties of materials used for specimen preparation

Properties	Steel tube	$CFRP_{Test}$	$GFRP_{Test}$	Adhesive [17]
Elastic Modulus (GPa)	211	75	23	3
Tensile Strength (MPa)	366	987	508	46
Yield Stress (MPa)	317	-	-	-
Thickness of FRP (mm)	-	0.52	0.49	-

Table 2 Details of impact test specimens

Specimen ID	FRP layers	FRP Type	Impact velocity (m/s)	FRP bond length (mm)
CFT-B-V1(1)	-	-	5.00	-
CFT-B-V1 (2)	-	-	5.00	-
CFT-B-V2	-	-	3.28	-
CCFT-L-V1	1	CFRP	5.00	1300
CCFT-H-V1	1	CFRP	5.00	1300
CCFT-LL-V1	2	CFRP	5.00	1300
CCFT-LL-V2	2	CFRP	3.28	1300
CCFT-LH-V1	2	CFRP	5.00	1300
CCFT-LLL-V1	3	CFRP	5.00	1300
CCFT-LHL-V1	3	CFRP	5.00	1300
GCFT-LL-V1	2	GFRP	5.00	1300
GCFT-HL-V1	2	GFRP	5.00	1300
GCCFT-LL-V1	2	GFRP+CFRP	5.00	1300
CCFT-LL1080-V1	2	CFRP	5.00	1080
CCFT-LL865-V1	2	CFRP	5.00	865
CCFT-LL650-V1	2	CFRP	5.00	650

Table 3 Impact test results

Specimen ID	H (m)	F_p (kN)	F_r (kN)	δ_p (mm)	δ_r (mm)	Displacement Record
CFT-B-V1(1)	1.27	268.4	85.0	87.0	79.2	Laser sensor
CFT-B-V1 (2)	1.27	266.0	80.0	86.4	78.8	Laser sensor
CFT-B-V2	0.55	182.6	75.0	40.0	31.0	Laser sensor
CCFT-L-V1	1.27	301.2	-	81.9	73.8	Video frames
CCFT-H-V1	1.27	307.6	85.0	81.1	65.3	Laser sensor
CCFT-LL-V1	1.27	250.4	90.0	76.5	65.3	Laser sensor
CCFT-LL-V2	0.55	165.6	95.0	30.5	20.0	Video frames
CCFT-LH-V1	1.27	248.3	82.0	80.6	71.1	Video frames
CCFT-LLL-V1	1.27	283.2	92.0	74.4	65.3	Video frames
CCFT-LHL-V1	1.27	248.9	87.0	72.7	65.3	Video frames
GCFT-LL-V1	1.27	315.9	87.0	75.1	64.8	Laser sensor
GCFT-HL-V1	1.27	302.9	87.0	75.7	65.3	Laser sensor
GCCFT-LL-V1	1.27	315.9	87.5	76.4	69.3	Laser sensor
CCFT-LL1080-V1	1.27	264.4	-	79.3	69.8	Video frames
CCFT-LL865-V1	1.27	290.3	-	82.6	77.0	Video frames
CCFT-LL650-V1	1.27	287.9	-	84.5	78.8	Video frames

Table 4. Absorption of impact energy due to global deformation

Specimen ID	Kinetic energy, E_k (kJ)	Dynamic capacity F_r (kN)	Global deformation energy, W_o (kJ)	$\frac{W_o}{E_k} \times 100\%$
CFT-B-V1 (2)	7.4	80	6.9	93.2
CFT-B-V2	3.2	75	3.0	93.8
CCFT-L-V1	7.4	-	-	-
CCFT-H-V1	7.4	85	6.9	93.2
CCFT-LL-V1	7.4	90	6.9	93.2
CCFT-LL-V2	3.2	95	2.9	90.6
CCFT-LH-V1	7.4	82	6.6	89.2
CCFT-LLL-V1	7.4	92	6.8	91.9
CCFT-LHL-V1	7.4	87	6.3	85.1
GCFT-LL-V1	7.4	87	6.5	87.8
GCFT-HL-V1	7.4	87	6.6	89.2
GCCFT-LL-V1	7.4	87.5	6.7	90.5